Hindawi Publishing Corporation
ISRN Robotics
Volume 2013, Article ID 593606, 8 pages
http://dx.doi.org/10.5402/2013/593606

Research Article

Internal and External Forces Measurement of Planar 3-DOF Redundantly Actuated Parallel Mechanism by Axial Force Sensors

Takashi Harada[1] and Podi Liu[2]

[1] *Kinki University, 3-4-1 Kowakae, Higashiosaka, Osaka 577-8502, Japan*
[2] *Graduate School of Science and Engineering, Kinki University, 3-4-1 Kowakae, Higashiosaka, Osaka 577-8502, Japan*

Correspondence should be addressed to Takashi Harada; harada@mech.kindai.ac.jp

Received 6 June 2013; Accepted 4 September 2013

Academic Editors: A. Bechar, F. Torres, and C. Zhu

This paper proposes a method for measuring the internal and external forces of a planar 3-DOF (degree of freedom) redundantly actuated parallel mechanism. The internal forces, force acts inside the endplate and mechanism constraint force, and the external forces, forces act on the endplate and thrusts by actuators, were measured simultaneously using the axial forces of the rods. Kinetostatic equations of the parallel mechanism were used to derive algorithms for measuring the internal and external forces. A link axis force sensor was developed using a strain gauge sensor. To verify the actual internal force of the endplate, a force sensor was also installed on the endplate. A real-time system for measuring the forces of the parallel mechanism was developed using RT-Linux. The external and internal forces were measured accurately.

1. Introduction

A robotic system with a parallel mechanism is mechanically characterized by high rigidity and precise positioning [1, 2]. However, the mechanical interactions and singularities of the mechanism restrict the workspace of the robot [3].

We previously proposed a 3-DOF (degree of freedom) ($xy\theta$) planar parallel mechanism with four redundant actuators [4–6]. This is aimed at a table mechanism with multi-axis machine tools. By developing a characteristic mechanical design, our mechanism avoids mechanical interactions around the links. The redundant actuation of the mechanism helps avoid singular configurations that would occur with nonredundant actuation. Our mechanism expands the workspace along the horizontal direction [4] and rotational motion [6]. Several studies have considered redundantly actuated 3-DOF planar parallel mechanisms [7–9]. However, these mechanisms were aimed at position control and not force control. Force control enables complex tasks such as the grinding and polishing of mechanical parts, which require a sensitive touch. We developed a novel design for a redundantly actuated parallel mechanism by using force-controlled linear motors and installing force command–based impedance control [5]. However, friction around the linear guide or force ripples of the linear actuators may adversely affect the accuracy of the force control. Sensing the actual forces and the moment at the tip of the mechanism is an effective method for improving the accuracy and stability of the force control [10].

Certain types of linearly actuated parallel mechanisms (e.g., the Stewart platform [1] and our parallel mechanism [4]) possess the distinct advantage of straightforward mapping expression between the wrenches (forces and moments) applied to the endplate and the forces applied to the rods of the mechanism. This advantage makes them particularly suitable for certain force sensor applications [11, 12]. For a redundantly actuated parallel mechanism, the internal forces act inside the endplate [8]. The internal force helps improve the mechanical rigidity and removes the backlash around joint pairs. Mimura et al. developed an internal force sensor that detects only the internal forces loaded inside the endplate [13]. Regardless of whether external and

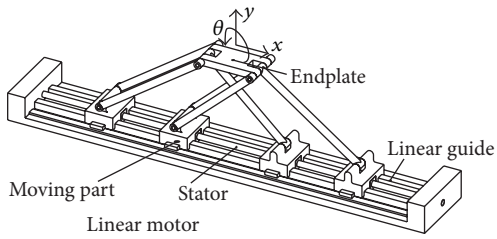

Figure 1: Conceptual design of planar parallel mechanism.

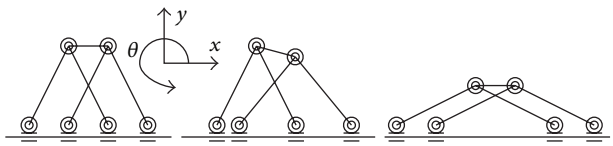

Figure 2: Motions of parallel mechanism.

internal forces both exist in the redundantly actuated parallel mechanism, conventional force sensing measures these forces not simultaneously but individually.

In this paper, we propose a novel method for simultaneously measuring the internal and external forces of a planar 3-DOF redundantly actuated parallel mechanism. The internal and external forces are measured simultaneously using the axial forces of the rods. The actual generated forces of the linear actuators and constraint forces at the driving pairs are measured by the system.

Algorithms for measuring the internal and external forces were derived by resolving the kinetostatic equations of the parallel mechanism. A link axis force sensor was developed using strain gauge sensors. To verify the actual internal force inside the endplate, a force sensor was also installed on the endplate. A system for measuring the forces in real-time was developed using RT-Linux. The external and internal forces of the parallel mechanism were measured accurately.

2. Simultaneous Measurement Method for External and Internal Forces

2.1. Redundantly Actuated Planar Parallel Mechanisms. Figures 1 and 2 depict the conceptual design and configuration, respectively, of the redundantly actuated 3-DOF parallel mechanism. Figure 3 shows the kinematic model of the mechanism. The end effector of the mechanism is set at the central position of the endplate.

2.2. Kinetostatics of Parallel Mechanism [14]. The differential kinematics or the relationship between the small displacements of the center of the end effector $\Delta\mathbf{P}$ and the small displacements of the controlled values of the actuators $\Delta\mathbf{c}$, is expressed as

$$\mathbf{J}_e\Delta\mathbf{p} = \mathbf{J}_c\Delta\mathbf{c},$$
$$\Delta\mathbf{p} = \left[\Delta x, \Delta y, \Delta\theta\right]^T, \qquad \Delta\mathbf{c} = \left[\Delta c_1, \ldots, \Delta c_4\right]^T. \tag{1}$$

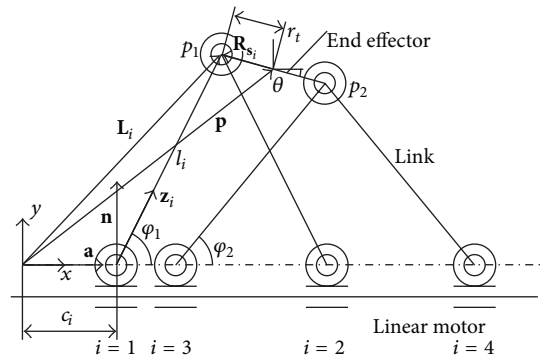

Figure 3: Kinematic model of planar parallel mechanism.

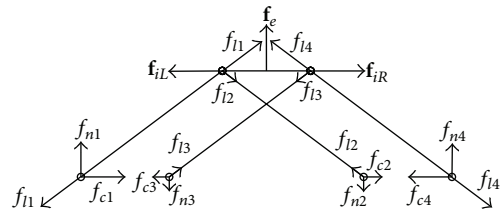

Figure 4: Internal and external forces of the planar parallel mechanism.

In (1), $\mathbf{J}_e$ and $\mathbf{J}_c$ are, respectively, 4×3 and 4×4 Jacobian matrices of the parallel mechanisms.

The relationship between the external forces $\mathbf{f}_e$, which act on the end effector of the mechanism, and actuator thrust forces $\mathbf{f}_c$ is derived as follows:

$$\mathbf{f}_e = \mathbf{J}_{ce}^T\mathbf{f}_c,$$
$$\mathbf{J}_{ce} = \mathbf{J}_c^{-1}\mathbf{J}_e, \tag{2}$$
$$\mathbf{f}_e = \left[f_x, f_y, \tau_\theta\right]^T, \qquad \mathbf{f}_c = \left[f_{c1}, \ldots, f_{c4}\right]^T.$$

In (2), $\mathbf{J}_{ce}$ is a 4×3 Jacobian matrix of the parallel mechanisms. As shown in Figure 4, f_{ni}, f_{li}, and f_{ci} are described as scalar values of the constraint force, axial force, and thrust force, respectively, acting on the node of the ith joint. The unit direction vector $\mathbf{a}$ along the direction of the thrust force is perpendicular to the unit direction vector $\mathbf{n}$ along the direction of the constraint force. The equilibrium equation of forces at the node of the ith joint is given by

$$f_{ci}\mathbf{a} + f_{ni}\mathbf{n} + f_{li}\mathbf{z}_i = 0. \tag{3}$$

The axial force and constraint force at each node are combined in vector form as $\mathbf{f}_l$ and $\mathbf{f}_n$, respectively. These forces are calculated from the actuator thrust force $\mathbf{f}_c$ as follows:

$$\mathbf{f}_l = -\mathbf{J}_c^{-1}\mathbf{f}_c,$$
$$\mathbf{f}_n = -\mathbf{J}_n\mathbf{f}_l = \left(\mathbf{J}_n\mathbf{J}_c^{-1}\right)\mathbf{f}_c. \tag{4}$$

In (4), $\mathbf{J}_n$ is a 4×4 Jacobian matrix that relates the axial forces $\mathbf{f}_l$ to the constraints forces $\mathbf{f}_n$. The internal forces $\mathbf{f}_{iR}$ and

$\mathbf{f}_{iL}$ act on the right and left pairs of the endplate, as shown in Figure 4. These vectors exist on the same line and have the same magnification but have opposite directions. The internal forces inside the endplate $\mathbf{f}_i$ are derived as follows:

$$\mathbf{f}_i = \left[\mathbf{f}_{iR} \;\; \mathbf{f}_{iL}\right]^T = f_i\left[\cos\theta \;\; \sin\theta \;\; -\cos\theta \;\; -\sin\theta\right]^T. \quad (5)$$

Equations (1)–(5) express basic relations for the internal forces (internal forces inside the endplate $\mathbf{f}_i$, constraint forces $\mathbf{f}_n$, and axial forces $\mathbf{f}_l$) and external forces (external forces acting on the end effector $\mathbf{f}_e$ and actuator thrust forces $\mathbf{f}_c$) of the parallel mechanism.

In our previous report on the impedance (force) control of the parallel mechanism [4], we derived the desired thrust forces $\mathbf{f}_c$ to realize the target external forces on the end effector $\mathbf{f}_e$ and target internal forces of the endplate $\mathbf{f}_i$ by solving (1)–(5) as follows:

$$\mathbf{f}_c = \left(\mathbf{J}_{ce}^T\right)^+ \mathbf{f}_e + \mathbf{J}_c^T \mathbf{J}_i^{-1} \mathbf{f}_i. \quad (6)$$

2.3. Measurement of Internal and External Forces. We measured the internal and external forces via the axial forces. By resolving (1)–(6), the internal forces (internal force inside the endplate $\mathbf{f}_i$ and constraint forces $\mathbf{f}_n$) and external forces (external forces acting on the end effector $\mathbf{f}_e$ and actuator thrust forces $\mathbf{f}_c$) of the parallel mechanism were measured using the axial forces $\mathbf{f}_l$. The Jacobian matrices $\mathbf{J}_c$ (4×4), $\mathbf{J}_e$ (4×3), $\mathbf{J}_n$ (4×4), and $\mathbf{J}_i$ (4×4) are given by the configuration of the parallel mechanism, and $\mathbf{J}_{ce}$ (4×3) is given by the second formula of (2).

The constraint forces $\mathbf{f}_n$ and actuator thrust forces $\mathbf{f}_c$ are measured from the axial forces $\mathbf{f}_l$ by resolving (4) for these forces as follows:

$$\begin{aligned} \mathbf{f}_n &= -\mathbf{J}_n \mathbf{f}_l, \\ \mathbf{f}_c &= -\mathbf{J}_c \mathbf{f}_l. \end{aligned} \quad (7)$$

By substituting the second formula of (7) into the first formula of (2), the external forces acting on the end effector $\mathbf{f}_e$ are measured from the axial forces $\mathbf{f}_l$ as follows:

$$\mathbf{f}_e = \mathbf{J}_{ce}^T \mathbf{f}_c = -\mathbf{J}_{ce}^T \mathbf{J}_c \mathbf{f}_l. \quad (8)$$

Equation (6) is rearranged, and the second formulas of (7) and (8) are substituted into it to obtain

$$\begin{aligned} \mathbf{J}_c^T \mathbf{J}_i^{-1} \mathbf{f}_i &= \mathbf{f}_c - \left(\mathbf{J}_{ce}^T\right)^+ \mathbf{f}_e \\ &= -\mathbf{J}_c \mathbf{f}_l + \left(\mathbf{J}_{ce}^T\right)^+ \mathbf{J}_{ce}^T \mathbf{J}_c \mathbf{f}_l \\ &= -\left(\mathbf{I} - \left(\mathbf{J}_{ce}^T\right)^+ \mathbf{J}_{ce}^T\right) \mathbf{J}_c \mathbf{f}_l. \end{aligned} \quad (9)$$

Equation (9) is used to determine the internal force inside the endplate $\mathbf{f}_i$ as follows:

$$\mathbf{f}_i = -\left(\mathbf{J}_c^T\right)^{-1} \mathbf{J}_i \left(\mathbf{I} - \left(\mathbf{J}_{ce}^T\right)^+ \mathbf{J}_{ce}^T\right) \mathbf{J}_c \mathbf{f}_l. \quad (10)$$

As shown in (7), (8), and (10), the internal forces (internal force inside the endplate $\mathbf{f}_i$ and constraint forces $\mathbf{f}_n$) and external forces (external forces acting on the end effector $\mathbf{f}_e$ and actuator thrust forces $\mathbf{f}_c$) of the parallel mechanism are measured by the axial forces $\mathbf{f}_l$.

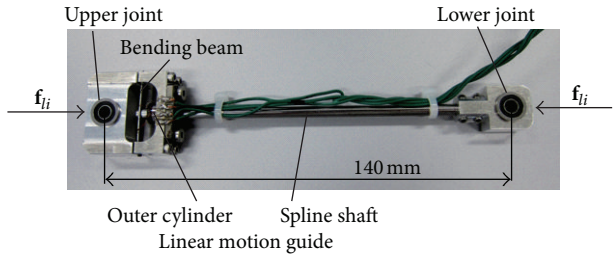

Figure 5: Link axis force sensor.

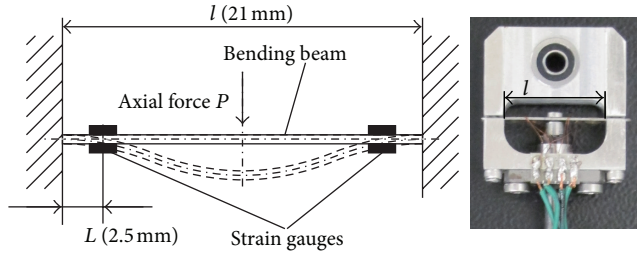

Figure 6: Dimensions of bending beam.

3. Design of Force Sensors

3.1. Design of Link Axis Force Sensor. The links of the planar mechanism are connected to the mechanical pairs by a pin joint. Therefore, only an axial force acts on each link. The design of the link axis force sensor is shown in Figure 5.

A linear motion guide supports the undesired load that is perpendicular to the link axis; this allows axial force to act almost ideally upon the bending beam. The axial force is measured as the strain ε of the bending beam by strain gauges attached to the beam. Figure 6 illustrates the model of the bending beam. The relationship between the axial force P and strain ε at the strain gauge location is given as follows:

$$\varepsilon = \frac{1}{ZE}\left(\frac{PL}{2}\left(\frac{1}{4} - \frac{L}{l}\right)\right). \quad (11)$$

In (11), Z and E represent the second moment of area and Young's modulus of the bending beam, respectively. The rated force capacity of the link axis sensor is designed to be 3.0 N as the rated thrust force of the linear actuator prototype is designed to be 2.25 N [5]. We designed the dimensions of the bending beam to generate a 1.0 microstrain when an axial force of 1.0 gf (0.01 N) acts along the link, as shown in Figure 6.

In the experiment, we produced four links with bending beam force sensors. The performances of the sensors were evaluated by increasing the compressive weights along the link in 50 gf (0.49 N) intervals from 0 to 300 gf (2.94 N) and then reducing the weights in 50 gf (0.49 N) intervals from 300 (2.94 N) to 0 gf. In the results, the linearity and hysteresis of the sensors became less than 1.5% and 2.0%, respectively. The output of each axial force sensor was calibrated by using the parameter of the least squared line fit to the data.

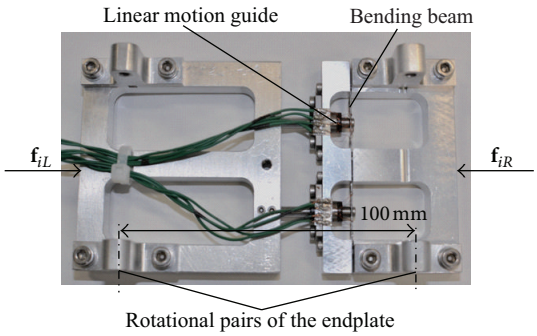

FIGURE 7: Sensor for internal force on endplate.

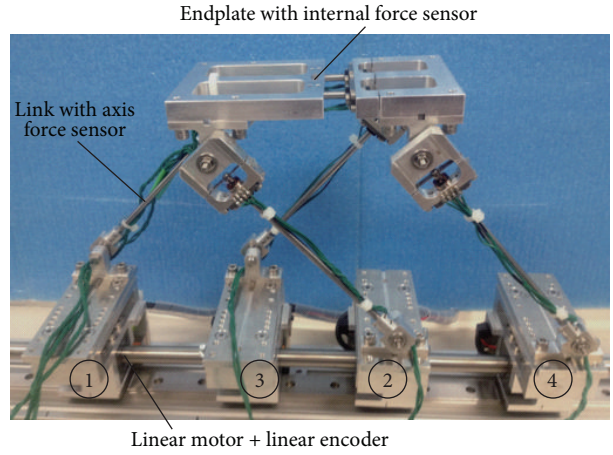

FIGURE 8: Parallel mechanism with force sensors.

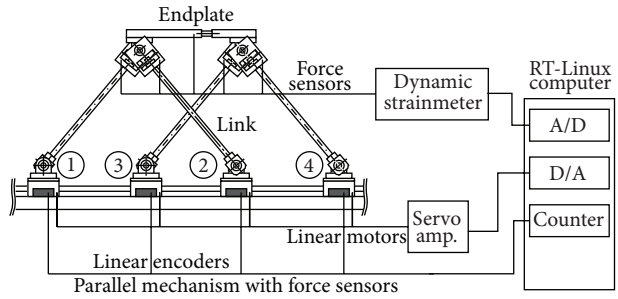

FIGURE 9: Schematic view of real-time measurement system.

This force sensor directory measures the link axis force $\mathbf{f}_l$. The internal forces $\mathbf{f}_i$ and $\mathbf{f}_n$ and the external forces $\mathbf{f}_e$ and $\mathbf{f}_c$ are indirectly measured using (7), (8), and (10).

3.2. Design of Internal Force Sensor on Endplate. The internal force on the endplate $\mathbf{f}_i$ is indirectly measured from the output values of the axis force sensors and (10). To validate these measurements, a force sensor that directly measures the internal force on the endplate was designed and built, as shown in Figure 7. Two bending beams and linear guides, which is the same design as that of the axis force sensor, were installed parallel to the same direction of the internal force on the endplate. The internal force on the endplate is directly measured as the sum of the two sensors.

The performance of the sensor was evaluated by increasing the compressive weight in 100 gf (0.98 N) intervals from 0 to 500 gf (4.9 N) and then reducing the weight in 100 gf (0.98 N) intervals from 500 (4.9 N) to 0 gf. In the results, the linearity and hysteresis of the sensor became less than 3.0% and 3.0%, respectively.

4. Development of Real-Time Measurement System

4.1. Redundantly Actuated Planar Parallel Mechanism with Force Sensors. The axial force sensors and sensor for the internal force on the endplate were installed on the redundantly actuated planar parallel mechanism, as shown in Figure 8.

4.2. Real-Time Measurement System. Figures 9 and 10 show the schematic and actual views, respectively, of the developed real-time measurement system. The measurement system used PC-Ubuntu8.10 RT-Linux (Linux kernel version: 2.6.29.1, Version 8 of RT patch). We developed the following two threads (procedures of programs).

(1) Measurement thread: The signals from the force sensors and linear encoders are read in the thread. The internal and external forces are calculated using (7), (8), and (10) in this thread.

(2) Drawing thread: The current configuration of the parallel mechanism is depicted on the computer screen by the OpenGL software in this thread. The internal and external forces are superimposed onto the picture of the parallel mechanism as graphical arrows and numerical values.

The measurement thread and drawing thread run simultaneously with time intervals of 3 and 10 ms, respectively. The values of the internal forces, external forces, and positions of the moving part of the linear motors are transferred from the measurement thread to the drawing thread via shared memory. Figure 11 shows an example execution screen of the real-time measurement system.

5. Evaluation of Force Measurement System

5.1. Evaluation of Accuracy of External Force Measurement. To evaluate the accuracy of external force measurement, given loads were added to the endplate of the parallel mechanism, as shown in Figure 12. We compared the actual load added on the endplate and the external forces measured by the real-time measurement system, while changing the configurations of the parallel mechanism, as shown in Figure 13. We added loads from 0 (0 N) to 500 gf (4.9 N) in

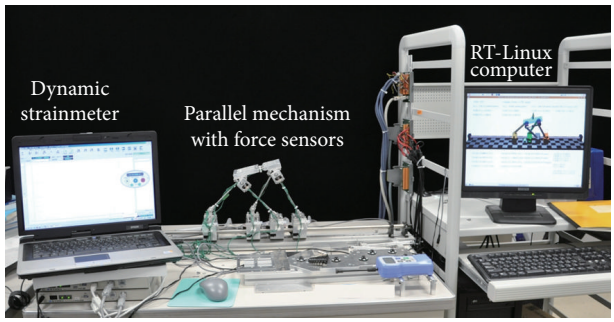

Figure 10: Actual view of real-time measurement system.

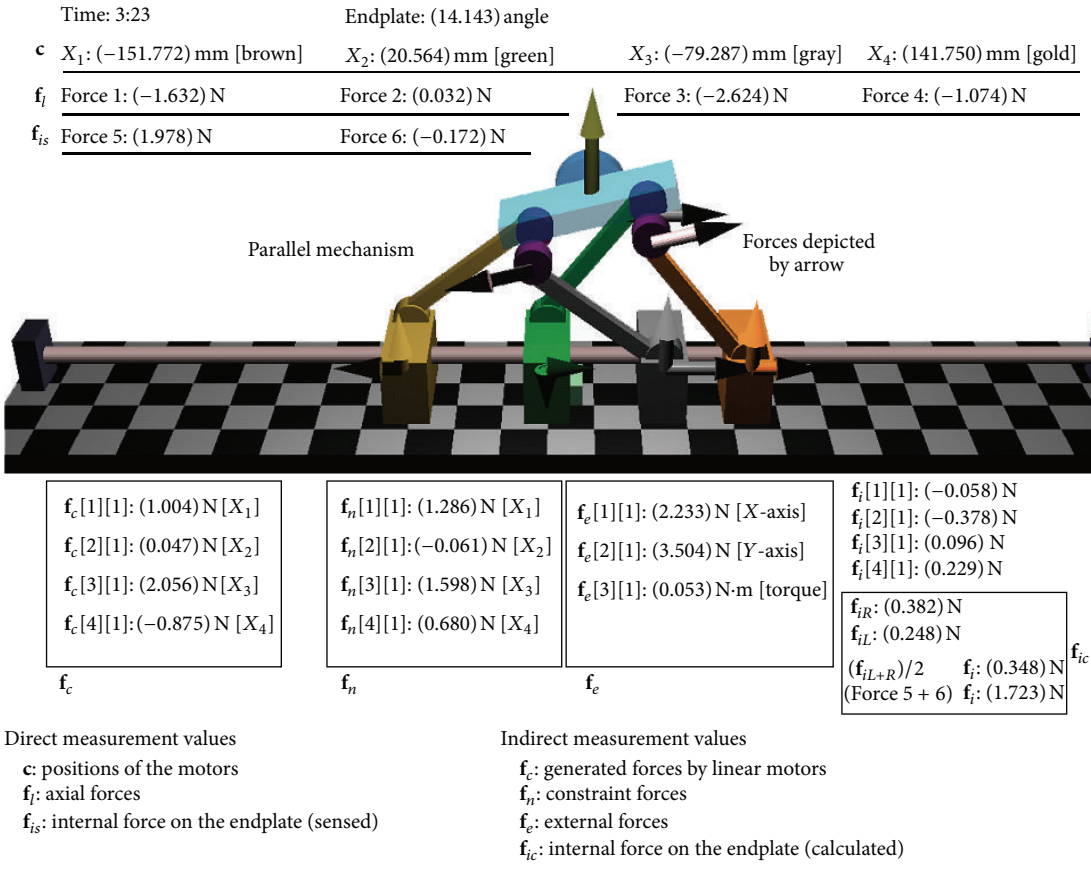

Figure 11: Execution screen of real-time measurement system.

intervals of 100 gf (0.98 N) loads to the x and y directions and added moments from 0 (0 N·m) to 25 kgf·mm (0.245 N·m) in intervals of 5 kgf·mm (0.049 N·m) to the rotational direction. Figure 14 shows an example of the experimental data for the force measurements.

We evaluated the force measurement accuracy according to the linearity (L) and sensitivity (S). The sensitivity of the force measurement was defined as the slope of the measured data. The ideal sensitivity (S) is equal to 1. As listed in Table 1, the linearity (L) of the external force measurement was less than 3.5%. The sensitivity of the external force measurements was 0.96–1.03.

5.2. Evaluation of Accuracy of Internal Force Measurement. As shown in Figure 15, given loads were added onto motor no. 4, whereas the other motors (nos. 1–3) were mechanically locked. Internal force inside the endplate was generated by the redundancy of the mechanism. We added loads from 0 (0 N) to 200 gf (1.96 N) in intervals of 50 gf (0.49 N) to motor no. 4 while changing the configurations of the parallel mechanism in the same manner as shown in Figure 13. Indirect measurement data from the axis force sensors and direct measurement data from the internal force sensor on the endplate were compared. Figure 16 shows an example of the experimental data on internal force measurements.

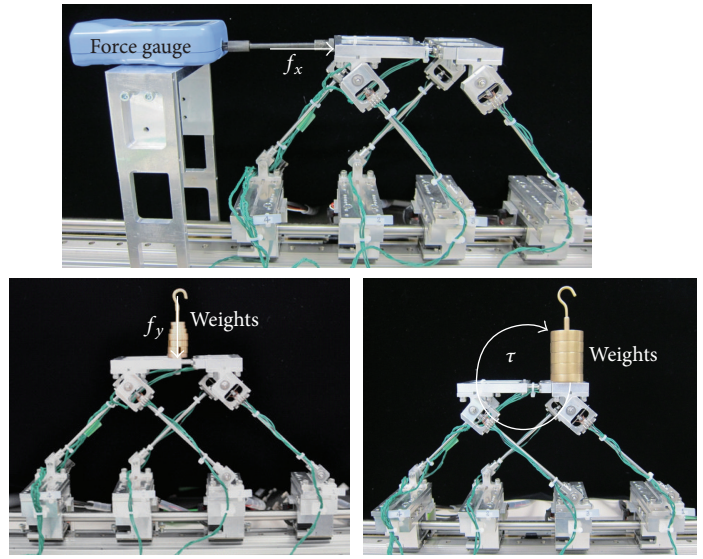

Figure 12: Experimental setup for evaluation of external force measurement.

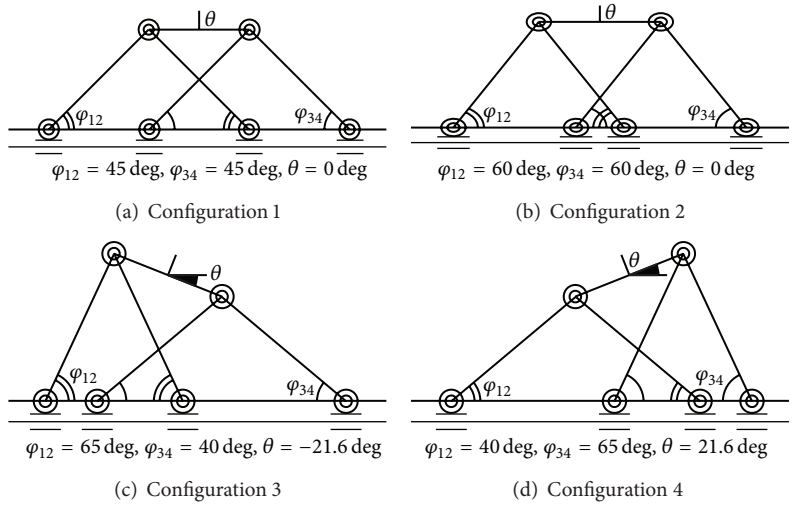

Figure 13: Configurations for evaluation of external force measurement.

Table 1: Experimental results for external force measurements.

Configuration	f_x		f_y		τ_θ	
	L	S	L	S	L	S
1	1.63%	0.99	1.76%	0.98	0.02%	1.00
2	1.43%	1.01	3.47%	1.03	0.04%	1.00
3	—	—	1.33%	1.01	—	—
4	—	—	3.39%	0.96	—	—

Table 2: Experimental results for internal force measurements.

Configuration	A_1	A_2	$(A_1 - A_2)/A_2$
1	1.06	1.11	−4.5%
2	1.93	1.91	1.0%
3	2.64	2.68	−1.5%
4	1.15	1.20	−4.2%

We evaluated the accuracy of the internal force measurement on the basis of the sensitivity (A). The sensitivity of the internal force measurement was defined as the slope of the measured data with respect to the added loads on the motor; that is, the sensitivity (A) coincided with the slope of the plot, as shown in Figure 16. The sensitivity of the indirect measurement data from the axis force sensors A_1, direct measurement data from the internal force sensor on the endplate A_2, and relative error between those values $(A_1 - A_2)/A_1$ are summarized in Table 2. The relative errors between the indirect measurement by the axis force sensors and direct measurement by the internal force sensor were from −4.5% to 1.0%.

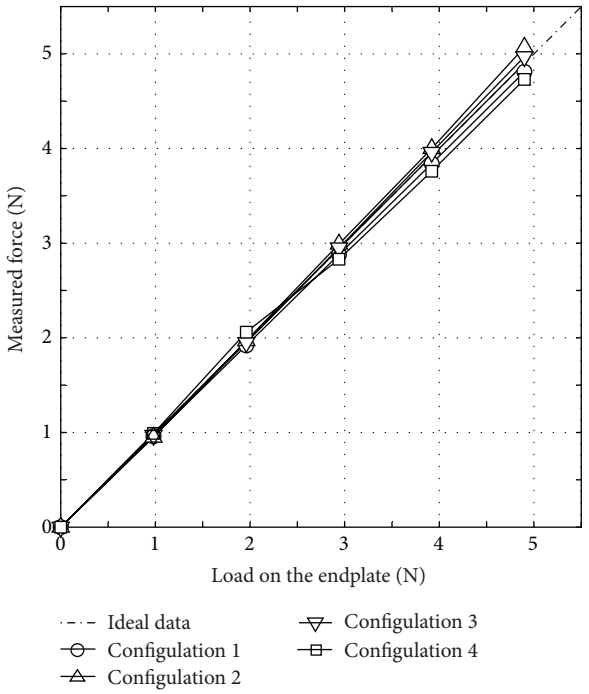

Figure 14: Experimental data for external force measurement of f_x.

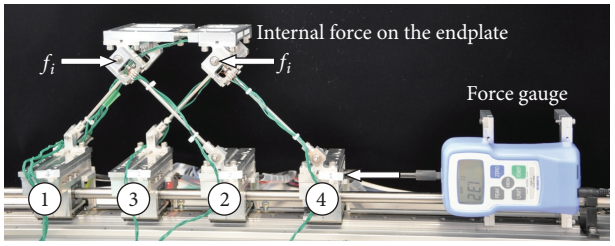

Figure 15: Experimental setup for evaluation of internal force measurement.

5.3. Discussion on Improving Measurement Accuracy. In the preliminary experiment, the axial force sensor had hysteresis caused by friction of the linear motion guide. The hysteresis was reduced by replacing the small friction linear motion guide. However, friction of the guide still remained and caused errors in the linearity of the axial force measurement.

There were dimension errors between the actual and ideal (modeled) mechanical parts. These errors occurred owing to the numerical errors in the Jacobian matrices of the parallel mechanism. Namely, the dimension errors produced sensitivity errors in the indirect force measurements that used (7), (8), and (10).

To improve the measurement accuracy, we will reduce the friction of the sliding parts and calibrate the kinematic parameters of the parallel mechanism.

6. Conclusion

We proposed a method for measuring the internal and external forces of a planar 3-DOF redundantly actuated parallel mechanism. These forces are simultaneously measured by the axial forces of the link. A link axis force sensor was fabricated to measure the external and internal forces of a 3-DOF planar redundant parallel mechanism. A real-time measurement system was developed using RT-Linux. The external and internal forces were accurately measured.

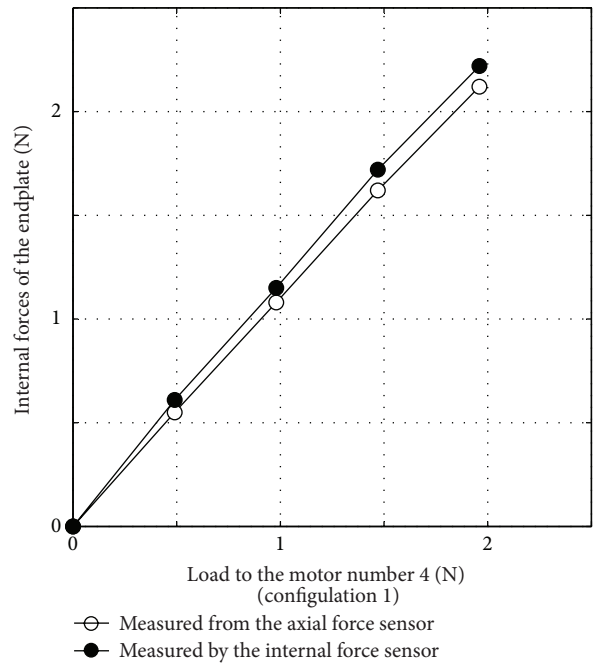

Figure 16: Experimental data for external force measurement of f_x.

Acknowledgments

This work was supported by JSPS KAKENHI Grant no. 80434851 and the MEXT-supported program for the strategic Research Foundation to Private Universities, 2012–2014.

References

[1] B. Dasgupta and T. S. Mruthyunjaya, "The stewart platform manipulator: a review," *Mechanism and Machine Theory*, vol. 35, no. 1, pp. 15–40, 2000.

[2] J. P. Merlet, *Parallel Robots*, Springer, 2006.

[3] J.-P. Merlet, "Singular configurations of parallel manipulators and Grassmann geometry," *International Journal of Robotics Research*, vol. 8, no. 5, pp. 45–56, 1989.

[4] T. Harada and M. Nagase, "Configurations and mathematical models of parallel link mechanisms using multi drive linear motors," in *Proceedings of the IEEE International Conference on Intelligent Robots and Systems (IROS '09)*, pp. 1974–1979, October 2009.

[5] T. Harada and M. Nagase, "Impedance control of a redundantly actuated 3-DOF planar parallel link mechanism using direct drive linear motors," in *Proceedings of the IEEE International Conference on Robotics and Biomimetics (ROBIO '10)*, pp. 501–506, December 2010.

[6] T. Uchikoshi and T. Harada, "Study of parallel mechanism with back-flip motion applying parallel drive system of linear

motors," in *Proceedings of the IEEE International Conference on Robotics and Biomimetics*, pp. 2002–2007, 2011.

[7] J. Wang, J. Wu, T. Li, and X. Liu, "Workspace and singularity analysis of a 3-DOF planar parallel manipulator with actuation redundancy," *Robotica*, vol. 27, no. 1, pp. 51–57, 2009.

[8] F. Marquet, S. Krut, O. Company, and F. Pierrot, "ARCHI: a new redundant parallel mechanism—modeling, control and first results," in *Proceedings of the IEEE International Conference on Intelligent Robots and Systems*, pp. 183–188, November 2001.

[9] X.-J. Liu, L. Guan, and J. Wang, "Kinematics and closed optimal design of a kind of PRRRP parallel manipulator," *Journal of Mechanical Design, Transactions of the ASME*, vol. 129, no. 5, pp. 558–563, 2007.

[10] T. Harada, Y. Nisida, H. Nagaoka, and N. Kimura, "Robust impedance control and its application to peg insertion," *Advanced Technologies in Robotics, Mechatronics and Manufacturing Systems*, pp. 339–344, 1993.

[11] R. Ranganath, P. S. Nair, T. S. Mruthyunjaya, and A. Ghosal, "A force-torque sensor based on a Stewart Platform in a near-singular configuration," *Mechanism and Machine Theory*, vol. 39, no. 9, pp. 971–998, 2004.

[12] J. Yao, Y. Hou, H. Wang, T. Zhou, and Y. Zhao, "Spatially isotropic configuration of Stewart platform-based force sensor," *Mechanism and Machine Theory*, vol. 46, no. 2, pp. 142–155, 2011.

[13] N. Mimura, R. Onodera, and A. Satani, "An internal force sensor for control of a redundant parallel manipulator," *Transactions of the Japan Society of Mechanical Engineers C*, vol. 72, no. 3, pp. 893–900, 2006 (Japanese).

[14] T. Harada, "Kinetostatics and dynamics of redundantly actuated planar parallel link mechanisms," *Numerical Analysis*, InTech, pp. 395–416, 2011.